https://doi.org/10.30799/jnst.376.26110505 J. Nanosci. Tech. - Volume 11 Issue 5 (2026) 1179–1184

ISSN: 2455-0191

Share Your Innovations through JACS Directory

Journal of Nanoscience and Technology

Visit Journal at https://www.jacsdirectory.com/jnst

Hydrothermal Design of Functional CeO_2 Nanomaterials for Efficient Visible-Light-Driven Photocatalytic and Antimicrobial Applications

Amruta M. Wagh[1], Sachin S. Kushare[2,*], Narendra U. Patil[1]

[1]Department of Physics, Material Research Lab., MVP Samaj's K.R.T. Arts, B.H. Commerce and A.M. Science (KTHM) College, Nashik – 422 002, MH, India.
[2]Department of Chemistry, Research Centre MVP Samaj's K.K. Wagh Arts, Science and Commerce College, Pimpalgaon (B) – 422 009, MH, India.

ARTICLE DETAILS

Article history:
Received 22 July 2026
Accepted 13 August 2026
Available online 23 August 2026

Keywords:
CeO_2
Hydrothermal
Dye Degradation
Antimicrobial Activity

ABSTRACT

Cerium oxide (CeO_2) nanoparticles (NPs) were synthesized using a hydrothermal method. The structural, morphological, optical, and surface properties of the synthesized nanoparticles were characterized by X-ray diffraction (XRD), scanning electron microscopy (SEM), UV–Visible spectroscopy (UV–Vis), Fourier transform infrared spectroscopy (FTIR), Raman spectroscopy, and Brunauer–Emmett–Teller (BET) surface area analysis. XRD analysis confirmed the formation of a cubic fluorite crystal structure with a space group of Fm-3m. The optical band gap energy of the CeO_2 nanoparticles, determined from UV–visible analysis, was found to be 2.85 eV. The photocatalytic activity of the synthesized nanoparticles was evaluated through the degradation of congo red (CR) dye under visible light irradiation. Complete degradation of congo red was achieved within 60 minutes of visible light exposure at room temperature under alkaline conditions (pH 10), demonstrating superior photocatalytic efficiency. The antimicrobial activity of the CeO_2 nanoparticles was investigated against *Escherichia coli*, *Candida albicans*, *Aspergillus niger*, and *Fusarium* spp. The results revealed significant antimicrobial activity against the tested microorganisms. Overall, the findings indicate that CeO_2 nanoparticles synthesized via the hydrothermal method exhibit excellent photocatalytic and antimicrobial properties, highlighting their potential as multifunctional materials for various environmental and biomedical applications.

1. Introduction

In recent years, cerium oxide (CeO_2) nanoparticles have attracted considerable attention due to their unique physicochemical properties and wide-ranging applications in materials science and nanotechnology. CeO_2 is a wide band gap semiconductor (3.19 eV) with excellent chemical stability, high thermal resistance, remarkable oxygen storage capacity, strong redox behavior (Ce^{3+}/Ce^{4+} transition), and notable catalytic activity [1-5]. Owing to these characteristics, CeO_2 has been extensively utilized in polishing agents, UV absorbers, fuel cells, gas sensors, photocatalysts, glass industries, cosmetics (sunscreens), and biomedical applications. At the nanoscale, CeO_2 exhibits enhanced surface reactivity, improved oxygen mobility, and size-dependent optical and electronic properties. These features make CeO_2 nanostructures promising candidates for electronic devices, antioxidant systems, antibacterial agents, and anticancer applications. The biological performance of CeO_2 nanoparticles strongly depends on particle size, morphology, surface chemistry, and biocompatibility [6-9]. Various synthesis techniques have been employed to fabricate CeO_2 nanostructures with controlled morphology and crystallinity, including co-precipitation, sol–gel processing, chemical vapor deposition, and hydrothermal methods. Among these, the hydrothermal approach is particularly advantageous due to its simplicity, cost-effectiveness, controlled crystal growth, high purity, and ability to tailor particle size and morphology under moderate reaction conditions [10-13].

Water pollution caused by untreated industrial wastewater remains a major global environmental challenge. Effluents containing dyes, pharmaceuticals, pesticides, surfactants, and heavy metals pose serious risks to aquatic ecosystems and human health. Semiconductor-based photocatalysis has emerged as a sustainable and cost-effective strategy for the degradation of such refractory pollutants [14-18]. Photocatalytic treatment under solar or visible light irradiation offers an environmentally friendly approach for wastewater remediation while potentially enabling simultaneous energy recovery. Metal oxide semiconductors, particularly titanium dioxide (TiO_2), have been widely studied as photocatalysts due to their chemical stability and non-toxicity. However, TiO_2 suffers from limitations such as a wide band gap requiring UV irradiation (which constitutes only 2–5% of solar radiation) and rapid recombination of photogenerated electron–hole pairs, leading to reduced photocatalytic efficiency [19-23]. CeO_2 has emerged as a promising alternative semiconductor photocatalyst. Its band gap ranges from 2.6 to 3.4 eV depending on synthesis conditions, allowing partial absorption in the visible region. Additionally, its high oxygen storage capacity, redox flexibility, and defect chemistry contribute to enhanced photocatalytic performance. The photocatalytic efficiency of CeO_2 can be further improved through morphology control, doping with metal or non-metal ions, semiconductor coupling, or hybridization with carbon-based materials [24-27].

Beyond photocatalysis, CeO_2 nanoparticles have demonstrated significant antimicrobial activity against bacteria, yeast, and fungi. The antibacterial mechanism is often attributed to electrostatic interactions between nanoparticles and microbial cell membranes, generation of reactive oxygen species (ROS), and oxidative stress-induced cellular damage [28-35]. Considering these advantages, the present study focuses on the hydrothermal synthesis of CeO_2 nanoparticles and a comprehensive investigation of their structural, morphological, and optical properties [36-42]. Furthermore, their photocatalytic performance toward dye degradation under visible light irradiation and their antimicrobial activity against selected microorganisms are systematically evaluated. The study aims to demonstrate the multifunctional potential of CeO_2 nanoparticles for environmental remediation and biomedical applications [43-45].

2. Experimental Methods

2.1 Materials

Cerium nitrate hexahydrate ($Ce(NO_3)_3{\cdot}6H_2O$), sodium hydroxide (NaOH), and polyethylene glycol (PEG) were procured from Aldrich Chemical Co. (Milwaukee, WI, USA). All chemicals were of analytical grade and used as received without further purification.

*Corresponding Author:sachinkushare7@gmail.com(Sachin S. Kushare)

https://doi.org/10.30799/jnst.376.26110505

Cite this Article as: Amruta M. Wagh, Sachin S. Kushare, Narendra U. Patil, Hydrothermal design of functional CeO_2 nanomaterials for efficient visible-light-driven photocatalytic and antimicrobial applications, J. Nanosci. Tech. 11(5) (2026) 1179–1184.

2.2 Synthesis of CeO_2 Nanoparticles

CeO_2 nanoparticles were synthesized via a template-free hydrothermal method by systematically varying the alkaline conditions, reaction time, and temperature. Initially, 0.1 M cerium nitrate hexahydrate was dissolved in distilled water under constant magnetic stirring for 30 min at room temperature to obtain a homogeneous solution. Subsequently, 0.5 N aqueous NaOH solution was added dropwise to the precursor solution under continuous stirring at room temperature. Thereafter, 1 mL of polyethylene glycol (PEG) was introduced into the reaction mixture while maintaining constant stirring to ensure uniform dispersion. The resulting homogeneous solution was transferred into a Teflon-lined stainless-steel autoclave, filling approximately 85% of its total volume. The sealed autoclave was then placed in an electric oven and maintained at 110 °C for 24 h to facilitate hydrothermal crystallization. After completion of the reaction, the autoclave was allowed to cool naturally to room temperature. The obtained precipitate was collected and thoroughly washed several times with distilled water and ethanol to remove residual impurities and unreacted species. The product was then dried and finely ground using a mortar and pestle to obtain ultrafine powder. Subsequently, the material was calcined at 800 °C for 5 hr to enhance the crystallinity and stability of the CeO_2 nanoparticles. The prepared CeO_2 nanoparticles were further utilized for photocatalytic degradation of congo red dye and for the evaluation of antimicrobial activity.

2.3 Characterization

The CeO_2 nanoparticle products were characterised using analytical methods. A Shimadzu 8400S FTIR spectrophotometer was used to analyse FTIR spectrum (KBr pellets) in the 4000 to 400 cm^{-1} range. The phase purity of the product was determined using an X-ray powder diffraction pattern utilising Rigaku Ultima IV copper equipment operating at 25 kV and 25 mA using CuK radiation with a wavelength of 0.154 nm and Bragg's scanning angle varying from 100 to 800. Using a scanning electron microscope (SEM) and FEI Nova Nano SEM 450 equipment, the material's surface shape and characteristics were verified. The Quantachrome Autosorb Automated Gas Sorption System Autosorb-1, NOVA-1200, and Mercury Porosimeter Autosorb-1c were used to determine the BET surface area using the N_2 adsorption–desorption isotherm.

2.4 Photocatalytic Degradation Experiments

The photocatalytic activity of CeO_2 nanoparticles was evaluated using the photocatalytic degradation of congo red dye under UV-visible light irradiation. Initially, three different kinds of perception were recorded. In the first test, 0.6 gm of CeO_2 nanoparticles were utilised as a photocatalyst to irradiate a 100 mL 5 mg/L solution of congo red dye in a photoreactor. The next trial was completed in the dark. In the third test, a photoreactor devoid of any catalyst was used to expose solely the congo red dye solution to UV-visible light. The degradation reaction was conducted with quantities of congo red dye in the range of 5–20 mg/L and varying amounts of generated photocatalyst, assuming time t=0. To separate suspended particles, enough aliquots were extracted at regular intervals and centrifuged for five minutes. The amount of congo red dye in the supernatant solution was then quantified using a UV-visible double beam spectrophotometer at the wavelength of absorbance maximum for congo red dye λ_{max} 500 nm. The percentage of dye degradation was calculated using an equation,

$$\% \text{ Degradation} = [(C_0 - C_t) / C0 \times 100] \quad (1)$$

where, C_0 is the initial concentration and C_t is the concentration after time.

3. Results and Discussion

3.1 X-Ray Diffraction Analysis (XRD)

The X-ray diffraction (XRD) pattern of the synthesized CeO_2 nanoparticles is presented in Fig. 1. The diffraction peaks observed at 2θ values of 28.55°, 33.06°, 47.59°, 56.33°, 59.02°, 69.40°, 76.86°, 79.11°, and 88.23° correspond to the characteristic reflections of crystalline cerium oxide. These peaks are indexed to the (111), (200), (220), (311), (222), (400), (331), and (420) crystallographic planes, respectively, confirming the formation of a cubic fluorite structure. The diffraction pattern is in good agreement with the standard data (JCPDS No. 34-0394), indicating the successful synthesis of phase-pure CeO_2 nanoparticles without detectable impurity phases. Furthermore, the hydrothermally synthesized sample exhibited relatively higher diffraction peak intensities compared to other samples, suggesting improved crystallinity and phase purity. The sharp and well-defined peaks further indicate the formation of highly crystalline CeO_2 nanoparticles [46]. The average crystallite size of the synthesized nanoparticles was estimated using the Debye–Scherrer equation, D= Kλ/ β Cos θ, where *D* represents the average crystallite size, *K* denotes the dimensionless shape factor (typically taken as 0.9), λ is the wavelength of the incident X-ray radiation (1.54 Å for Cu Kα), *β* corresponds to the full width at half maximum (FWHM) of the selected diffraction peak (in radians), and *θ* is the Bragg diffraction angle. The calculated average crystallite size of the synthesized CeO_2 nanoparticles was determined to be approximately 6.736 nm, indicating the formation of nanocrystalline cerium oxide.

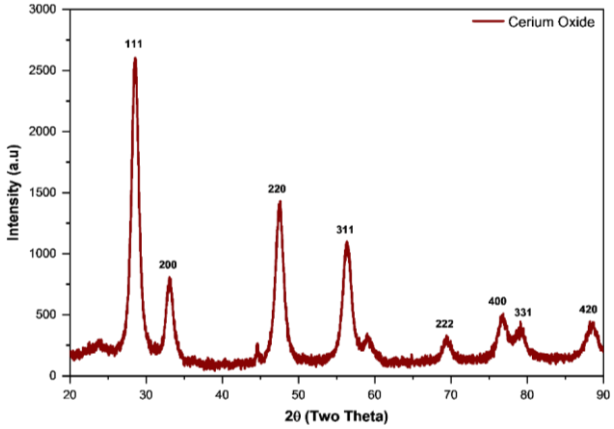

Fig. 1 XRD pattern of synthesised CeO_2 nanoparticles

3.2 UV–Visible Spectroscopy Analysis

The optical absorption properties of the synthesized cerium oxide (CeO_2) nanoparticles were investigated using UV–visible spectroscopy. Fig. 2(a) illustrates the variation of optical absorbance as a function of wavelength. The optical absorption coefficient (α) was evaluated within the wavelength range of 300–800 nm. The UV–vis absorption spectrum exhibits a distinct absorption edge at approximately 339 nm, which corresponds to the fundamental band gap absorption of CeO_2 nanoparticles.

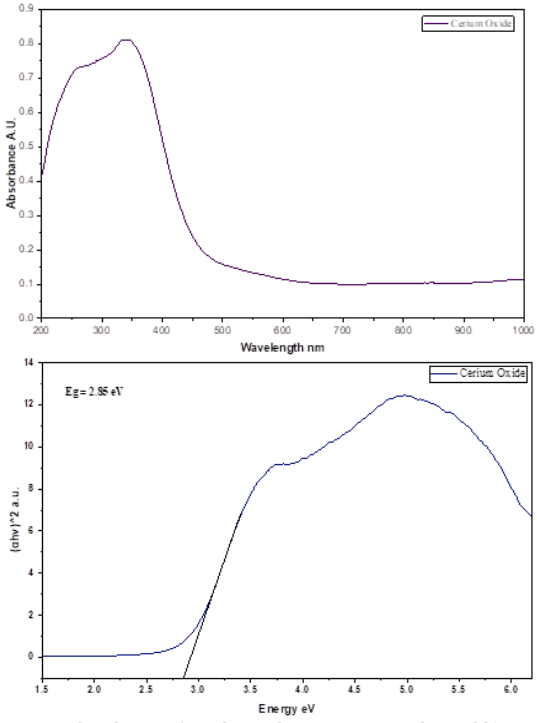

Fig. 2 a) UV-vis absorbance of synthesised CeO_2 nanoparticles and b) Tauc plot of Synthesised CeO_2 nanoparticles

The optical absorption coefficient (α) was calculated from the transmittance data using the following relation [47].

$$\alpha = 1/d \log (1/T) \quad (2)$$

where T is the transmittance and d is the thickness. The study has an absorption coefficient (α) obeying the following relation for high photon energies (hν).

https://doi.org/10.30799/jnst.376.26110505

Cite this Article as: Amruta M. Wagh, Sachin S. Kushare, Narendra U. Patil, Hydrothermal design of functional CeO_2 nanomaterials for efficient visible-light-driven photocatalytic and antimicrobial applications, J. Nanosci. Tech. 11(5) (2026) 1179–1184.

$$\alpha = A\,(h\nu - Eg)^{1/2}/h\nu \quad (3)$$

In the above relation, α represents the absorption coefficient, denotes the optical band gap energy, and *A* is a proportionality constant. The fundamental absorption arises from electronic transitions between the valence band and the conduction band, which can be employed to determine both the nature and magnitude of the optical band gap of the synthesized nanoparticles. To evaluate the direct optical band gap, a Tauc plot was constructed by plotting $(\alpha h\nu)^2$ as a function of photon energy (hν), as illustrated in Fig. 2(b). The band gap energy was determined by extrapolating the linear region of the plot to the photon energy axis at $(\alpha h\nu)^2 = 0$. The optical band gap of the synthesized CeO_2 nanoparticles was calculated to be 2.85 eV.

3.3 Functional Group Analysis using FT-IR Spectroscopy

The Fourier transform infrared (FTIR) spectrum of the synthesized cerium dioxide (CeO_2) nanoparticles is shown in Fig. 3. The functional groups present in the sample were identified by analyzing the absorption bands within the wavenumber range of 400–4000 cm^{-1}. The spectral features obtained confirm the formation of CeO_2 and reveal the presence of surface-associated functional groups [48]. Distinct absorption bands at 640.46 cm^{-1}, 499.62 cm^{-1}, and 415.60 cm^{-1} are attributed to the Ce-O stretching vibrations, which verify the formation of cerium oxide. The band observed at 1057.66 cm^{-1} is assigned to Ce–O–Ce bridging vibrations within the crystal lattice. The absorption band centered at 1618.6 cm^{-1} corresponds to the bending vibration mode of adsorbed water molecules (H–O–H). Furthermore, the broad band at 3393.97 cm^{-1} is associated with O–H stretching vibrations arising from surface hydroxyl groups and/or physically adsorbed water molecules. Overall, the FTIR analysis confirms the successful synthesis of CeO_2 nanoparticles and indicates the presence of surface hydroxyl functionalities.

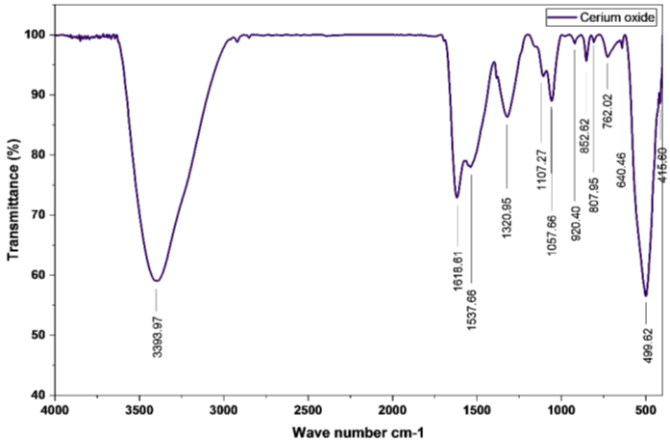

Fig. 3 FTIR of synthesised CeO_2 nanoparticles

3.4 SEM and EDAX Analysis

The morphological characteristics of CeO_2 nanoparticles were systematically investigated using scanning electron microscopy (SEM), and their elemental composition was determined via energy-dispersive X-ray spectroscopy (EDAX). SEM analysis revealed that the synthesized powders are highly porous and consist of densely packed aggregates of nanosized particles. These primary nanoparticles are predominantly spherical and exhibit a narrow and uniform size distribution, indicating controlled nucleation and growth during the synthesis process. It is well-established that as the particle size of nanomaterials decreases, the surface-to-volume ratio increases dramatically. Consequently, nanoparticles exhibit high surface energy, making them thermodynamically unstable in their isolated state.

To minimize the total surface energy, nanoparticles spontaneously aggregate and form clusters, a phenomenon known as agglomeration. The degree of agglomeration typically increases with decreasing particle size due to stronger van der Waals interactions and other surface forces between particles [49].

CeO_2 nanoparticles possess additional unique features that enhance agglomeration. Specifically, they can form coherent interfaces where the crystal lattices of adjacent particles align in a lattice-matched configuration. This alignment reduces the interfacial energy and stabilizes the aggregate structure. Such coherent interfaces are energetically favourable and represent a mechanism by which ceria nanoparticles minimize overall system energy. This is very important for CeO_2, as its fluorite crystal structure allows for facile lattice matching between particles, facilitating strong, stable agglomerates (Fig. 4a).

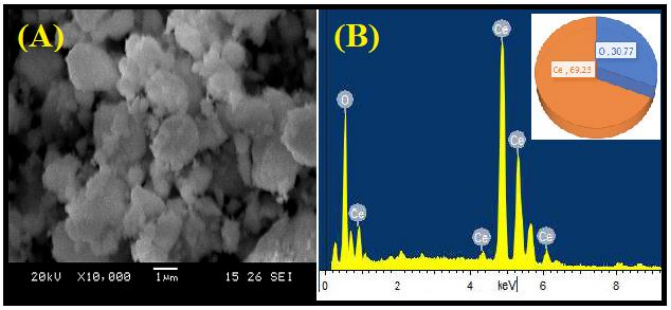

Fig. 4 (a) SEM images and (b) EDAX images and elemental composition of CeO_2

EDAX characterization confirmed the elemental composition of the nanoparticles, showing the exclusive presence of cerium (Ce) and oxygen (O) (Fig. 4b). No extraneous peaks were detected in the spectra, indicating the absence of contaminants and confirming the high chemical purity of the as-synthesized CeO_2 nanoparticles [50]. The purity is critical for applications such as catalysis and fuel cells, where even trace impurities can significantly alter surface reactivity and electronic properties.

3.5 Raman Spectroscopy

The structural characteristics of the synthesized CeO_2 nanoparticles were further investigated using Raman spectroscopy, as depicted in Fig. 5. The Raman spectrum of the as-prepared cerium oxide nanoparticles exhibits a prominent and sharp peak at 462 cm^{-1}. This peak is assigned to the F_2g Raman-active vibrational mode, which is characteristic of the fluorite-type cubic crystal structure of CeO_2. The F_2g mode arises from the symmetric stretching vibrations of the Ce-O bonds within the CeO_2 lattice, reflecting the integrity and uniformity of the oxygen sublattice in the fluorite framework. The intensity and sharpness of this Raman band indicate a high degree of crystallinity, suggesting that the nanoparticles are well-ordered at the atomic scale. Raman spectroscopy is particularly sensitive to local structural distortions, oxygen vacancies, and defects in metal oxides. The absence of additional peaks or significant shifts in the spectrum confirms that the synthesized CeO_2 nanoparticles possess a pure and defect-minimized fluorite cubic structure, consistent with X-ray diffraction results. Thus, the Raman analysis provides complementary confirmation of the crystallographic phase and high structural quality of the as-prepared nanoparticles [51].

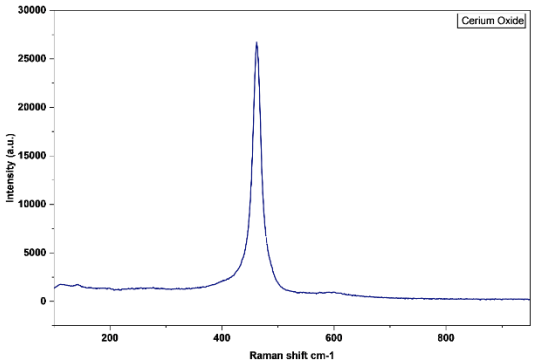

Fig. 5 Raman spectra of syntheised CeO_2 nanoparticles

3.6 Brunauer–Emmett–Teller (BET) Surface Analysis

The BET surface area analysis of synthesized CeO_2 revealed a specific surface area of 66170 cm^2/g, with a pore volume of 0.008 cc/g and an average pore diameter of 1.811 nm (Table 1). The pore diameter (<2 nm) indicates a microporous structure according to IUPAC classification. The low pore volume suggests limited internal porosity, likely due to particle agglomeration during synthesis. Although the textural properties indicate moderate surface development, the catalytic performance of CeO_2 is primarily governed by its oxygen vacancies and the reversible Ce^{3+}/Ce^{4+} redox couple, which enhance its oxygen storage and redox behaviour.

Table 1 BET surface area, pore volume, and pore diameter of CeO_2 nanoparticle

Material	Surface area (cm^2/g)	Pore Volume (cc/g)	Pore Diameter (nm)
CeO_2	66170	0.008	1.811

3.7 Photocatalytic Degradation Study of Synthesized Nanoparticles

The photocatalytic degradation efficiency of the produced distinct CeO_2 nanoparticles was investigated using the photodegradation of congo red

https://doi.org/10.30799/jnst.376.26110505

Cite this Article as: Amruta M. Wagh, Sachin S. Kushare, Narendra U. Patil, Hydrothermal design of functional CeO_2 nanomaterials for efficient visible-light-driven photocatalytic and antimicrobial applications, J. Nanosci. Tech. 11(5) (2026) 1179–1184.

dye. Using a double beam spectrophotometer, absorbance was measured every five minutes to examine the photodegradation of congo red dye. CeO_2 (0.4 g) nanoparticles are used as a photocatalyst in the congo red dye photodegradation of dye (5 mg/L). In the absence of a photocatalyst, Fig. 6 demonstrates that exposing a dye solution (5 mg/L) to visible light has no effect on absorbance. The absorbance of congo red dye is unaffected by the presence of CeO_2 nanoparticles in the dark and in the absence of UV-visible light, but a very slight shift in absorbance is noted. Third investigations show that congo red dye (5 mg/L) degrades when exposed to visible light in the presence of CeO_2 (0.6 g) nanoparticles acting as a photocatalyst.

In conclusion, only 0.6 g of CeO_2 nanoparticle shows improved photocatalytic activity for congo red dye discolouration and mineralisation. The absorbance at the characteristic wavelength of CR was recorded, and the corresponding dye concentration at time t was denoted as Ct. The photocatalytic degradation efficiency (η) was calculated using the following formula,

$$\% \text{ degradation}, \eta = (C_0 - C_t)/C_0 \times 100 \quad (4)$$

where C_0 is the initial dye concentration and Ct is the concentration at time t [52].

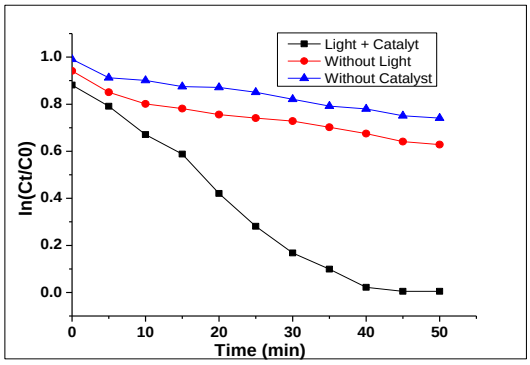

Fig. 6 Effect of catalyst and light irradiation on dye degradation

3.8 Optimization Study Photocatalytic Degradation of Congo Red Dye

3.8.1 Effect of Dye Concentration

The impact of dye concentration to assess the CeO_2 nanoparticles' photocatalytic degradation efficiency. Congo red dye was utilised as an organic contaminant, as seen in Fig. 7. Three synthetic photocatalysts were tested for their capacity to degrade congo red dye at different starting concentrations (5–20 mg/L). CeO_2 nanoparticles shown enhanced percentage 99% degradation of congo red dye (5 mg/L) in just 60 minutes when the light was turned on for the appropriate amount of time. The continuous colour fading of congo red dye about time under the light was caused by CeO_2. This is attributed to improved structural and optical qualities because of the appropriate band position and increased surface area brought about by the successful unique shape.

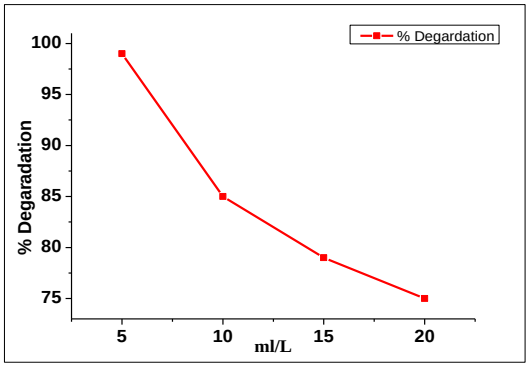

Fig. 7 Effect of initial dye concentration on the photocatalyst degradation of congo red by using CeO_2 nanoparticles

3.8.2 Effect of Catalyst Dose

An essential component of researching the photocatalytic degradation of congo red dye is simplifying the photocatalyst. The number of CeO_2 nanoparticles (0.2–0.8 g) in the presence of UV or visible light with a solution of congo red dye (5 mg/L) is shown in Fig. 8. The degradation efficiency rises to 0.6 g as the photocatalyst concentration rises. Catalyst saturation in the dye solution, which causes uneven catalyst dispersion throughout the dye solution and less degradation, is most likely the cause of the reduced proficiency. Furthermore, photodegradation is reduced when catalyst concentration is increased.

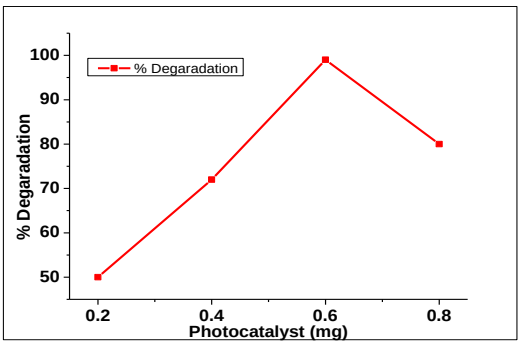

Fig. 8 Effect of amount of photocatalyst on congo red dye degradation

The degradation rate decreases with increased addition because photons are dispersed from the photocatalyst's surface. The lowest concentration of CeO_2 nanoparticles identified in this study was 0.6 g per 100 mL at 5 mg/L. Congo red dye mixture. The breakdown of dye before and after exposure to visible light and photocatalyst is shown in Fig. 9. As the irradiation time rises, the dark red colourization of the congo red dye solution is completely reduced by the chromophoric absorption peak at 500 nm. The solution's colour (absorbance 500 nm) significantly decreased, indicating that the absorbance reaches a minimum in 60 minutes when CeO_2 nanoparticles are present.

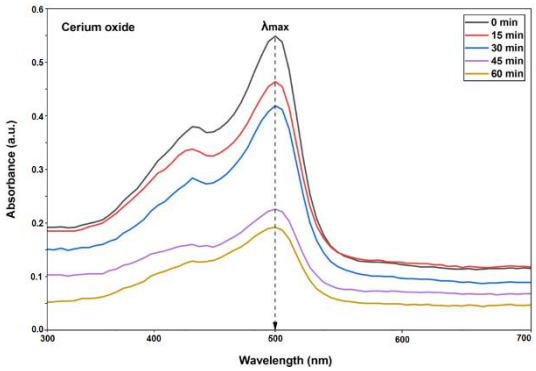

Fig. 9 UV–Visible spectrum of dye before and after degradation using CeO_2 nanoparticles

3.8.3 Effect of pH on Dye Degradation

The effect of pH on the photocatalytic degradation of congo red dye was investigated under visible light irradiation. The experiments were carried out using an initial dye concentration of 5 mg/L and a photocatalyst dosage of 0.6 g, while the pH of the solution was varied at 4, 6, 8, and 10 (Fig. 10) The results revealed that the degradation efficiency of CR dye strongly depends on the pH of the reaction medium. Among the studied conditions, the maximum degradation efficiency was observed at pH 8. This enhanced performance at slightly alkaline pH may be attributed to improved adsorption of dye molecules on the catalyst surface and the increased generation of reactive oxygen species (•OH radicals), which facilitate the photocatalytic degradation process. At lower or higher pH values, the degradation efficiency decreased, possibly due to changes in the surface charge of the photocatalyst and reduced interaction between the dye molecules and the catalyst surface.

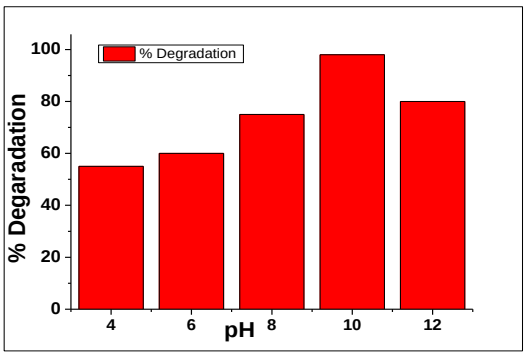

Fig. 10 Effect of pH of photocatalyst on congo red dye degradation

https://doi.org/10.30799/jnst.376.26110505

Table 2 Comparative study of photocatalytic dye degradation using modified CeO_2 nanoparticles under visible light

S. No.	Nano-particles	Dye	Degradation %	Time
1	Cerium oxide	Congo Red	97.7%	130 min [53]
2	CeO2/S-GCN	Congo Red	64.8 %	120 min [54]
3	Cu-doped CeO_2	Congo Red	98%	35 min [55]
4	Cerium oxide	Indigo carmine	90%	180 min [56]
5	La doped CeO_2	Congo Red	98%	35 min [57]
6	Ni doped CeO2	Methylene blue	85.83%	120 min [58]
7	CeO_2	Congo Red	99%	60 min (This work)

Table 2 summarizes the photocatalytic degradation of various dyes using composite and doped CeO_2 nanoparticles under visible light irradiation reported in previous studies. Compared with these reported materials, the CeO_2 nanoparticles synthesized in the present work show promising degradation efficiency toward congo red dye.

3.9 Antimicrobial Activity

The antimicrobial activity of the synthesized cerium oxide nanoparticles (CeO_2 NPs) was investigated against selected bacterial and fungal strains, including *Escherichia coli*, *Candida albicans*, *Aspergillus niger*, and *Fusarium* spp. The bacterial strain (*E. coli*) was cultured on nutrient agar (NA) medium, while the fungal strains (*C. albicans, A. niger*, and *Fusarium* spp.) were cultured on Sabouraud Dextrose Agar (SDA) medium. All microbial cultures were incubated at 37 °C for 24 hr to ensure optimal growth. For the antimicrobial assay, freshly prepared microbial suspensions were uniformly inoculated into 100 mL of sterilized NA and SDA media, which were then poured into sterile petri dishes and allowed to solidify. The synthesized CeO_2 nanoparticles were dispersed in sterile distilled water to prepare a nanoparticle suspension with a concentration of 20 mg/mL, followed by sonication to ensure uniform dispersion. Sterile distilled water at a concentration of 100 mg/mL was used as a negative control to verify that no inhibition occurred in the absence of nanoparticles. The antimicrobial activity was evaluated using the agar diffusion method under visible light irradiation conditions. After applying the CeO_2 NP suspension onto the inoculated agar plates, the petri dishes were incubated in a visible light irradiation reactor at 37 °C for 24 hr. During incubation, the interaction between the nanoparticles and microbial cells under visible light was expected to enhance antimicrobial effects through the generation of reactive oxygen species (ROS).

Table 2 Antimicrobial activity of CeO_2 nanoparticles

Bacteria/Fungus	Zone of Inhibitions (mm)
Escherichia. Coli	9.3
Candida albicans	12
Aspergillus niger	12.6
Fusarium spp	10.6

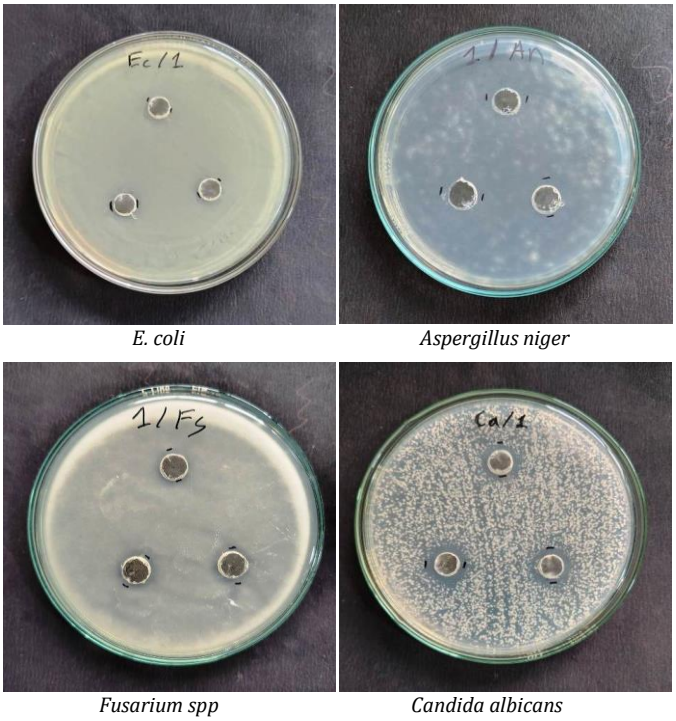

E. coli *Aspergillus niger*

Fusarium spp *Candida albicans*

Fig. 11 Antimicrobial activity of CeO_2 nanoparticles

Following incubation, the antimicrobial efficacy of the CeO_2 nanoparticles was assessed by measuring the diameter of the inhibition zones formed around the treated areas. The zones of inhibition were measured in millimetres (mm) using a calibrated scale, and the average inhibition zone diameter was calculated to determine the relative antimicrobial activity of the synthesized nanoparticles against the tested microorganisms. The comparative antimicrobial activity of the synthesized CeO_2 nanoparticles against different microbial pathogens is illustrated in Fig. 11, while the corresponding zones of inhibition are summarized in Table 2. The results demonstrate that the antimicrobial efficiency of CeO_2 nanoparticles varies depending on the type of microorganism. Among the tested pathogens, *Aspergillus niger* exhibited the most pronounced susceptibility, showing a larger zone of inhibition than the other microbial strains. This enhanced inhibition may be attributed to the effective interaction between CeO_2 nanoparticles and the fungal cell membrane, leading to structural damage and increased generation of reactive oxygen species (ROS), which disrupt essential cellular functions. In contrast, the other tested microorganisms displayed relatively lower inhibition zones, indicating comparatively reduced sensitivity toward the synthesized nanoparticles. These findings suggest that CeO_2 nanoparticles possess significant antifungal potential, particularly against *Aspergillus niger*.

4. Conclusion

Cerium oxide nanoparticles (CeO_2 NPs) were successfully synthesized using a hydrothermal method. The crystalline structure and phase formation of the synthesized nanoparticles were confirmed by X-ray diffraction (XRD) analysis, The morphology and particle size distribution of the cerium oxide nanoparticles were further examined using scanning electron microscopy (SEM) coupled with energy dispersive X-ray spectroscopy (EDS). The SEM images indicated the nanoscale morphology of the particles, while the EDS analysis confirmed the presence of cerium and oxygen as the major elements, demonstrating the high purity of the synthesized CeO_2 nanoparticles without detectable impurities. The crystalline nature of the prepared nanoparticles was further supported by the XRD and SEM analyses. Fourier Transform Infrared (FT-IR) spectroscopy revealed characteristic vibrational bands corresponding to Ce-O stretching, confirming the formation of cerium oxide nanoparticles. Raman spectroscopic analysis further verified the structural characteristics and indicated the predominantly spherical morphology of the CeO_2 nanoparticles.

The optical properties of the synthesized nanoparticles were investigated using UV–visible absorption spectroscopy. Photocatalytic activity studies demonstrated efficient degradation of congo red dye under visible light irradiation. Complete degradation of the dye was achieved within 60 minutes using 0.6 g of CeO_2 catalyst at pH 10 with a dye concentration of 5 mg/L at room temperature. These results indicate that cerium oxide nanoparticles exhibit significant potential for the treatment and purification of coloured wastewater generated from textile and other industrial sources. Furthermore, the photocatalytic efficiency and functional properties of CeO_2 nanoparticles can be further enhanced through various modifications such as dopant incorporation. In addition, the synthesized nanoparticles demonstrated effective antimicrobial activity, suggesting their promising applicability in biomedical and environmental applications.

References

[1] H. Li, F. Meng, J. Gong, Z. Fan, R. Qin, Structural, morphological and optical properties of shuttle-like CeO_2 synthesized by a facile hydrothermal method, J. Alloys Compd. 722 (2017) 489–498.

[2] K. Negi, M. Kumar, G. Singh, S. Chauhan, M.S. Chauhan, Nanostructured CeO_2 for selective-sensing and smart photocatalytic applications, Ceram. Int. 44 (2018) 15281–15289.

[3] H.A. Gate, Effect of high temperature on thermal analysis, structure and morphology of CeO_2 nanoparticles prepared by hydrothermal method, Int. J. Thin Film Sci. Technol. 11 (2022) 201–206.

[4] M.S. Pujar, S.M. Hunagund, D.A. Barretto, V.R. Desai, S. Patil, S.K. Vootla, A.H. Sidarai, Synthesis of cerium-oxide NPs and their surface morphology effect on biological activities, Bull. Mater. Sci. 43 (2020) 24.

[5] R. Suresh, V. Ponnuswamy, R. Mariappan, Effect of annealing temperature on the microstructural, optical and electrical properties of CeO_2 nanoparticles by chemical precipitation method, Appl. Surf. Sci. 273 (2013) 457–464.

[6] W.A. Aboutaleb, R.A. El-Salamony, Effect of Fe_2O_3-CeO_2 nanocomposite synthesis method on the congo red dye photodegradation under visible light irradiation, Mater. Chem. Phys. 236 (2019) 121724.

[7] F. Caputo, M. Mameli, A. Sienkiewicz, S. Licoccia, F. Stellacci, L. Ghibelli, E. Traversa, A novel synthetic approach of cerium oxide nanoparticles with improved biomedical activity, Sci. Rep. 7 (2017) 4636.

https://doi.org/10.30799/jnst.376.26110505

Cite this Article as: Amruta M. Wagh, Sachin S. Kushare, Narendra U. Patil, Hydrothermal design of functional CeO_2 nanomaterials for efficient visible-light-driven photocatalytic and antimicrobial applications, J. Nanosci. Tech. 11(5) (2026) 1179–1184.

[8] C.H. Hu, C.H. Xia, F. Wang, M. Zhou, P.F. Yin, X.Y. Han, Synthesis of Mn-doped CeO_2 nanorods and their application as humidity sensors, Bull. Mater. Sci. 34 (2011) 1033–1037.

[9] A. Mari, M.V. Vincent, D. Pachiyappan, R. Mookkaiah, U. Sambath, Structural, optical and photocatalytic properties of cerium oxide nanoparticles, Nanochem. Res. 10 (2025) 1–8.

[10] V. Shah, S. Shah, H. Shah, F.J. Rispoli, K. McDonnell, S. Workeneh, et al., Antibacterial activity of polymer coated cerium oxide nanoparticles, PLoS ONE 7 (2012) e47827.

[11] S.S. Kushare, V.D. Bobade, V.N. Suryawanshi, Synthesis and characterization of novel $CoCr_2O_4$@GeO_2@ZnO core–shell nanostructure: Focus on electrical conductivity and gas sensing properties, J. Inorg. Organomet. Polym. Mater. 32 (2022) 2679–2695.

[12] A.V. Borhade, V.D. Bobade, D.R. Tope, A highly selective and sensitive H_2S gas sensor based on novel nanostructure core–shell $FeCr_2O_4$@ZnO@MgO, J. Inorg. Organomet. Polym. Mater. 31 (2021) 4670–4683.

[13] A.V. Borhade, D.R. Tope, S.S. Kushare, Fly ash supported NiO as an efficient catalyst for the synthesis of xanthene and its molecular docking study against *Plasmodium glutathione* reductase, Res. Chem. Intermed. 44 (2018) 7459–7478.

[14] I. Celardo, J.Z. Pedersen, E. Traversa, L. Ghibelli, Pharmacological potential of cerium oxide nanoparticles, Nanoscale 3 (2011) 1411–1420.

[15] S.S. Kushare, V.D. Bobade, D.R. Tope, A.V. Borhade, $CoCr_2O_4$@GeO_2@ZnO core-shell nanoparticle as a novel recoverable catalyst: Preparation, characterization and photocatalytic degradation of basic fuchsin dye, J. Indian Chem. Soc. 98 (2021) 100239.

[16] A.V. Borhade, D.R. Tope, J.A. Agashe, S.S. Kushare, Synthesis, characterization and photocatalytic study of $FeCr_2O_4$@ZnO@MgO core-shell nanoparticle, J. Water Environ. Nanotechnol. 6 (2021) 164–176.

[17] A. Borhade, D. Tope, S. Kushare, Mercenaria shell powder as a cost-effective and eco-friendly photocatalyst for the degradation of Eriochrome Black T dye, Iran. J. Sci. Technol. Trans. Sci. 44 (2020) 75–83.

[18] T. Masui, K. Fujiwara, K.I. Machida, G.Y. Adachi, T. Sakata, H. Mori, Characterization of cerium (IV) oxide ultrafine particles prepared using reversed micelles, Chem. Mater. 9 (1997) 2197–2204.

[19] A. Fazal, J. Tariq, I. Javed, A. Ishaq, M.S.H. Naqvi, M. Maaza, Facile synthesis of ferromagnetic Ni-doped CeO_2 nanoparticles with enhanced anticancer activity, Appl. Surf. Sci. 357 (2015) 931–936.

[20] A. Rianjanu, A.S.P. Mustamin, E. Kartini, A. Melati, R. Aflaha, et al., Photocatalytic degradation of aqueous congo red dye pollutants by rare-earth metal oxide (CeO_2) nanorods, Colloids Surf. A Physicochem. Eng. Asp. 682 (2024) 132919.

[21] S.M.L. Dos, R.C. Lima, C.S. Riccardi, R.L. Tranquilin, P.R. Bueno, J.A. Varela, et al., Preparation and characterization of ceria nanospheres by microwave-hydrothermal method, Mater. Lett. 62 (2008) 4509–4511.

[22] L.P. Oana, D. Zorit¸a, M. Amalia, V. Dan, C. Lucian, C. Lelia, et al., FT-IR studies of cerium oxide nanoparticles and natural zeolite mater, Bull. Food Sci. Technol. 72 (2015) 50–55.

[23] K.J. Jasmine, A.N. Samson, Synthesis of CeO_2 nanoparticles by chemical precipitation and the effect of a surfactant on the distribution of particle sizes, J. Ceram. Process. Res. 12 (2011) 74–79.

[24] E. Varga, P. Pusztai, L. Ovari, A. Oszko, A. Erdohelyi, C. Papp, et al., Probing the interaction of Rh, Co and bimetallic Rh-Co nanoparticles with the CeO_2 support catalytic materials for alternative energy generation, Phys. Chem. Chem. Phys. 17 (2015) 27154–27166.

[25] M.J. Munoz-Batista, M. Fernandez-Garcia, A. Kubacka, Promotion of CeO_2-TiO_2 photoactivity by g-C_3N_4: Ultraviolet and visible light elimination of toluene, Appl. Catal. B Environ. 164 (2015) 261–270.

[26] M.J. Munoz-Batista, M.A. Nasalevich, T.J. Savenije, F. Kapteijn, J. Gascon, A. Kubacka, M. Fernandez-Garcia, Enhancing promoting effects in g-C_3N_4-Mn^{n+}/CeO_2-TiO_2 ternary composites: Photo-handling of charge carriers, Appl. Catal. B Environ. 176–177 (2015) 687–698.

[27] Y. Yu, Q. Zhong, W. Cai, J. Ding, Promotional effect of N-doped CeO_2 supported CoOx catalysts with enhanced catalytic activity on NO oxidation, J. Mol. Catal. A Chem. 398 (2015) 344–352.

[28] D. Sharma, B.R. Mehta, Nanostructured TiO_2 thin films sensitized by CeO_2 as an inexpensive photoanode for enhanced photoactivity of water oxidation, J. Alloys Compd. 749 (2018) 329–335.

[29] D. Sharma, V.R. Sastsangi, R. Shrivastav, U.V. Waghmare, S. Dass, Understanding the photoelectrochemical properties of nanostructured CeO_2/CuO_2 heterojunction photoanode for efficient photoelectrochemical water splitting, Int. J. Hyd. Ener. 41 (2016) 18339–18350

[30] D. Yin, F. Zhao, L. Zhang, X. Zhang, Y. Liu, et al., Greatly enhanced photocatalytic activity of semiconductor CeO_2 by integrating with upconversion nanocrystals and graphene, RSC Adv. 6 (2016) 103795–103802.

[31] C. Zhang, X. Zhang, Y. Wang, S. Xie, Y. Liu, X. Lu, Y. Tong, Facile electrochemical synthesis of CeO_2 hierarchical nanorods and nanowires with excellent photocatalytic activities, New J. Chem. 38 (2014) 2581–2586.

[32] D. Channei, B. Inceesungvorn, N. Wetchakun, S. Ukritnukun, A. Nattestad, J. Chen, S. Phanichphant, Photocatalytic degradation of methyl orange by CeO_2 and Fe-doped CeO_2 films under visible light irradiation, Sci. Rep. 4 (2014) 5757.

[33] J. Saranya, K.S. Ranjith, P. Saravanan, D. Mangalaraj, R.T.R. Kumar, Cobalt-doped cerium oxide nanoparticles: Enhanced photocatalytic activity under UV and visible light irradiation, Mater. Sci. Semicond. Process. 26 (2014) 218–224.

[34] R. Li, C. Li, S. Yin, C. Fu, T. Satom, Synthesis of C-N Co-doped nano-CeO_2 and dye degradation under compact fluorescent lamp irradiation, J. Nanosci. Nanotechnol. 12 (2012) 2797–2801.

[35] M. Mittal, A. Gupta, O.P. Pandey, Role of oxygen vacancies in Ag/Au doped CeO_2 nanoparticles for fast photocatalysis, Sol. Energy 165 (2018) 206–216.

[36] Z. Xiu, Z. Xing, Z. Li, X. Wu, X. Yan, et al., Ti^{3+}-TiO_2/Ce^{3+}-CeO_2 nanosheet heterojunctions as efficient visible-light-driven photocatalysts, Mater. Res. Bull. 100 (2018) 191–197.

[37] X. Qu, D. Xie, L. Gao, F. Du, Synthesis and photocatalytic activity of TiO_2/CeO_2 core-shell nanotubes, Mater. Sci. Semicond. Process. 26 (2014) 657–662.

[38] S. Issarapant, K. Wetchakun, S. Phanichphant, W. Kangwansupamokon, N. Wetchakun, A novel CeO_2/Bi_2WO_6 composite with highly enhanced photocatalytic activity, Mater. Lett. 156 (2015) 28–31.

[39] K. Huang, Y.H. Li, C. Liang, X. Xu, Y.F. Zhou, et al., One-step synthesis of reduced graphene oxide-CeO_2 nanocubes composites with enhanced catalytic activity, Mater. Lett. 124 (2014) 223–226.

[40] W. Wang, Q. Zhu, Q. Dai, X. Wang, Fe-doped CeO_2 nanosheets for catalytic oxidation of 1,2-dichloroethane: Effect of preparation method, Chem. Eng. J. 307 (2017) 1037–1046.

[41] X.J. Yu, P.B. Xie, Q.D. Su, Size-dependent optical properties of nanocrystalline CeO_2:Er obtained by combustion synthesis, Chem. Phys. 3 (2011) 5266–5269.

[42] N. Zhang, G. Zhang, S. Chong, H. Zhao, T. Huang, J. Zhu, Ultrasonic impregnation of MnO_2/CeO_2 and its application in catalytic sono-degradation of methyl orange, J. Environ. Manage. 205 (2018) 134–141.

[43] A.I.Y. Tok, F.Y.C. Boey, Z. Dong, X.L. Sun, Hydrothermal synthesis of CeO_2 nanoparticles, J. Mater. Process. Technol. 190 (2007) 217–222.

[44] I.D. Yadav, A. Ansari, D. Yadav, S.S. Garje, Facile synthesis of CeO_2 nanoparticles and their applications in photodegradation of methylene blue and as supercapacitor electrode material, Bull. Mater. Sci. 46 (2023) 86.

[45] K.B. Kusuma, M. Manju, C.R. Ravikumar, N. Raghavendra, M.A. Shilpa Amulya, et al., Photocatalytic degradation of Methylene Blue and electrochemical sensing of paracetamol using Cerium oxide nanoparticles synthesized via sonochemical route, Appl. Surf. Sci. Adv. 11 (2022) 100304.

[46] F.M. Meng, L.N. Wang, J.B. Cui, Controllable synthesis and optical properties of nano-CeO_2 via a facile hydrothermal route, J. Alloys Compd. 556 (2013) 102–108.

[47] C. Zhang, F.M. Meng, L.N. Wang, M. Zhang, Z.L. Ding, Morphology-selective synthesis method of gear-like CeO_2 microstructures and their optical properties, Mater. Lett. 130 (2014) 202–205.

[48] N.S. Arul, D. Mangalaraj, P.C. Chen, N. Ponpandian, P. Meena, Y. Masuda, Enhanced photocatalytic activity of cobalt-doped CeO_2 nanorods, J. Sol-Gel Sci. Technol. 64 (2012) 515–523.

[49] N. Thovhogi, A. Diallo, A. Gurib-Fakim, M. Maaza, Green synthesis of CeO_2 nanoparticles using *Moringa oleifera* plant extract and their antimicrobial activity, J. Alloys Compd. 647 (2015) 392–396.

[50] D. Suresh, P.C. Nethravathi, H. Rajanaika, H. Nagabhushana, S.C. Sharma, Green synthesis of multifunctional CeO_2 nanoparticles using plant extract and their catalytic activity, Mater. Sci. Semicond. Process. 31 (2015) 446–454.

[51] P. Singh, R. Kumar, A. Sharma, Structural, optical, and Raman spectroscopic investigation of cerium oxide nanoparticles synthesized by a hydrothermal method, Ceram. Int. 49 (2023) 4567–4575.

[52] X. Li, Y. Zhang, L. Chen, H. Wang, Enhanced photocatalytic degradation of organic dyes using defect-engineered CeO_2 nanostructures under visible light irradiation, J. Environ. Chem. Eng. 11 (2023) 109245.

[53] S. Kumar, P. Sharma, J. Singh, Green synthesis of cerium oxide nanoparticles and their photocatalytic and antimicrobial applications, Colloids Surf. A Physicochem. Eng. Asp. 670 (2023) 132919.

[54] R. Kumar, P. Singh, A. Sharma, Photocatalytic degradation of organic pollutants using metal oxide nanomaterials for wastewater treatment applications, J. Water Process Eng. 63 (2025) 108052.

[55] Y. Zhang, H. Liu, X. Wang, L. Chen, Defect engineering in cerium oxide nanostructures for enhanced photocatalytic and antibacterial performance, Nanotechnol. 35 (2024) 205701.

[56] A. Ali, H. Zafar, M. Zia, I.U. Haq, A.R. Phull, J.S. Ali, A. Hussain, Synthesis, characterization, applications, and challenges of iron oxide nanoparticles, AIMS Mater. Sci. 7 (2020) 468–488.

[57] Y. Zhang, X. Wang, H. Liu, L. Chen, Defect engineering in cerium oxide nanostructures for enhanced photocatalytic and antibacterial performance, Nanotechnol. 35 (2024) 205701.

[58] A. Kumar, R. Singh, P. Sharma, Photocatalytic degradation of organic pollutants using semiconductor nanomaterials for renewable energy and environmental remediation, Results Eng. 16 (2022) 100664.

https://doi.org/10.30799/jnst.376.26110505

Cite this Article as: Amruta M. Wagh, Sachin S. Kushare, Narendra U. Patil, Hydrothermal design of functional CeO_2 nanomaterials for efficient visible-light-driven photocatalytic and antimicrobial applications, J. Nanosci. Tech. 11(5) (2026) 1179–1184.